Journal of Electroceramics, 13, 261–265, 2004
© 2004 Kluwer Academic Publishers. Manufactured in The Netherlands.

Study of Microwave Dielectric Properties of Perovskite Thin Films by Near-Field Microscopy

YI-CHUN CHEN,[1,3] YUN-SHUO HSIEH,[1] HSIU-FUNG CHENG[1,*] & I-NAN LIN[2]

[1] *Department of Physics, National Taiwan Normal University, Taipei 116, Taiwan, Republic of China*
[2] *Department of Physics, Tamkang University, Tamsui 251, Taiwan, Republic of China*
[3] *Institute of Physics, Academia Sinica, Taipei 115, Taiwan, Republic of China*

Submitted February 13, 2003; Revised February 5, 2004; Accepted February 5, 2004

Abstract. Perovskite thin film materials possess good dielectric properties, which vary with applied voltage, and have thus been thoroughly investigated for applications as thin film tunable microwave devices. However, the tunability of the thin film materials derived from the frequency response of the thin film devices suffers from ambiguity in extracting the true dielectric response of the thin film materials in microwave frequency regime. To circumvent such a difficulty, we investigated the dielectric properties of perovskite thin films by using a novel scanning evanescent microwave microscopy (SEMM). To extract the dielectric parameters from original microwave frequency response signal of SEMM probe, we perform a 3-dimensional (3D) finite element simulation to model the frequency behavior of the SEMM microwave probe. Dielectric images of the thin films with submicron resolution can be obtained by using such a near-field technique, which correlates very well with the morphology of the films examined by atomic force microscopy. Moreover, the dielectric images of dielectric thin films were compared to those of ferroelectric thin films in order to discuss the related dielectric mechanism of the materials.

Keywords: scanning evanescent microwave microscopy, perovskite, tunable thin films

1. Introduction

Ferroelectric thin films possess several advantages over bulk materials, including (1) lower operation voltage, (2) faster response and (3) nonlinear relationship in dielectric properties, which increases the tunability [1–5]. Much attention has been paid to the application of ferroelectric thin films, such as (Ba, Sr)TiO_3 (BST), Pb(Zr,Ti)O_3 (PZT), $PbTiO_3$ (PT), and $(Pb_{1-x}La_x)TiO_3$ (PLT) for tunable microwave device, such as planar capacitors, waveguides, phase shifters, tunable mixers and filters [6–9]. Among the ferroelectric ceramics, the PZT materials, which possess a wide range of ferroelectric properties depending on the cationic ratio, have been extensively applied in electro-optic devices. The same desirable dielectric properties are expected in thin film form. However, the microwave dielectric properties of a thin film are very difficult to be accurately measured, which is restricted by the classical limit that the spatial resolution of any instrument based on the propagation of electromagnetic fields is $\lambda/2$. A novel measuring technique, which can directly evaluate the microwave dielectric properties of a thin film is thus urgently needed.

Over the years, a variety of near-field scanning microscope have been developed to probe local variations of properties and the structures of materials, and the spatial resolutions of $\lambda/20$–$\lambda/600$ [10]. An evanescent microwave probe (EMP) based on a microwave resonator [11–14] is proposed to image surface impedance profiles with high resolution, and spatial resolution is further improved to ~50 nm by using a tip-probe and efficient shielding structure. In this study, we investigate the dielectric properties of Pb(Zr,Ti)O_3 (PZT), thin films, by using EMP

*To whom all correspondence should be addressed. E-mail: hfcheng@phy03.phy.ntnu.edu.tw

technique. For comparison, the microwave dielectric materials, $Ba(Mg_{1/3}Ta_{2/3})O_3$ [15, 16], BMT, which exhibit especially low dielectric loss in microwave frequency region, are also studied in the form of thin films. A 3D finite element simulation is performed to solve the complexity of the electric field distribution in the tip-sample region.

2. Experimental Methods

The PZT thin films were prepared by metal-organic decomposition (MOD) process, the precursors containing proper proportion of $Pb(C_7H_{15}COO)_2$, $Zr(C_7H_{15}COO)_4$ and $Ti(OC_2H_5)_2(C_9H_{19}COO)_2$ were dissolved in xylene, with or without the addition of nano-PZT powders. The concentration of powder-less Pb-Zr-Ti precursors is 0.3 M, whereas that of the nano-PZT (0.05 M) containing precursors is reduced to 0.25 M to maintain the total PZT-content for the precursors the same. The Pb-Zr-Ti precursors were then spin-coated on a Pt-coated (200 nm) Si (100), containing a thin Ti-coating (50 nm) underneath the Pt-film as adhesion layer, followed by pyrolysis at 400°C for 30 min. Thus obtained dry films were then furnace annealed (FA) at 550 and 600°C (60 min) in air to convert the amorphous films into crystalline phase. The BMT thin films were prepared by a 2-step pulsed laser deposition (PLD) process using a KrF excimer laser ($\lambda = 248$ nm, Lambda Physik) with an energy density of 7 J/cm^2. The films were first deposited at 200°C in 0.08 mbar Po_2 for 30 min, followed by post-annealing at 600°C in air for 60 min. The structure of the films was analyzed using X-ray diffractometry (XRD, Rigaku D/max-II) and the morphology of the films were examined using scanning electron microscope (SEM, Joel JSM-840A).

An evanescent microwave probe was used to make nondestructive measurements of the dielectric properties of the films. The system design consists of a sharpened metal tip mounted on the center conductor of the $\lambda/4$ coaxial resonator with high-Q (quality factor), protruding beyond an aperture formed on the endwall of the resonator. A sapphire disk with a center hole of size close to the diameter of the tip wire ~50–100 μm and a metal layer (~1 μm) coating on the outside surface was used to shield off the far-field propagating components. This design minimizes the far-field background signal and allows submicron spatial resolution even in the quantitative analysis of complex dielectric constant. The resonator acts both as an evanescent field emitter and a detector. A change in the local environment of the probe leads to a change in resonance frequency f_0 of the resonator, and the signal is detected by measuring the power response near the resonant frequency. Moreover, since the field intensity at the tip increases as the tip sharpens, most energy radiated from the tip is absorbed by the sample nearby significantly. Due to the favorable field distribution caused by tip-probe (radius $R_0 \sim$ 10–100 μm), a small change in field distribution near the tip induces a large change in f_0, and high spatial resolution and high sensitivity are obtained.

3. Results and Discussions

In order to investigate the dielectric properties of thin films in the microwave frequency region, the EMP technique was introduced. Figure 1(a) illustrates schematically the EMP apparatus, which includes a micro-tip extended from a coaxial resonator for guiding the evanescent wave into the samples. The resonant system of EMP can be analyzed using a lumped series resonant circuit, and tip-sample interaction is equivalent by a capacitance:

$$C_{\text{tip-sample}} = C_r + iC_i, \tag{1}$$

where C_r and C_i are the real and imaginary parts of the tip-sample capacitance, which are contributed from the dielectric constant K and dielectric loss tanδ (or $1/Q$) of the tested sample, respectively. In general, due to the rapid decay of the evanescent wave, the tip-sample capacitance is far less than the resonator capacitance, so perturbation theory could be used to analyze the resonant system. Given measured resonant frequency f_r and quality factor Q, the complex tip-sample capacitance can be extracted from:

$$\frac{\Delta f}{f_0} = \frac{f_r - f_0}{f_0} = -\frac{C_r}{2C}, \tag{2}$$

$$\Delta\left(\frac{1}{Q}\right) = \frac{1}{Q} - \frac{1}{Q_0} = -\left(\frac{1}{Q_0} + \frac{2C_i}{C_r}\right)\frac{\Delta f}{f_0}, \tag{3}$$

where f_0 and Q_0 are the resonant frequency and quality factor of the resonator respectively, when there is no sample near the tip.

The most general approach to determine the effective tip-sample capacitance is to apply an exact finite

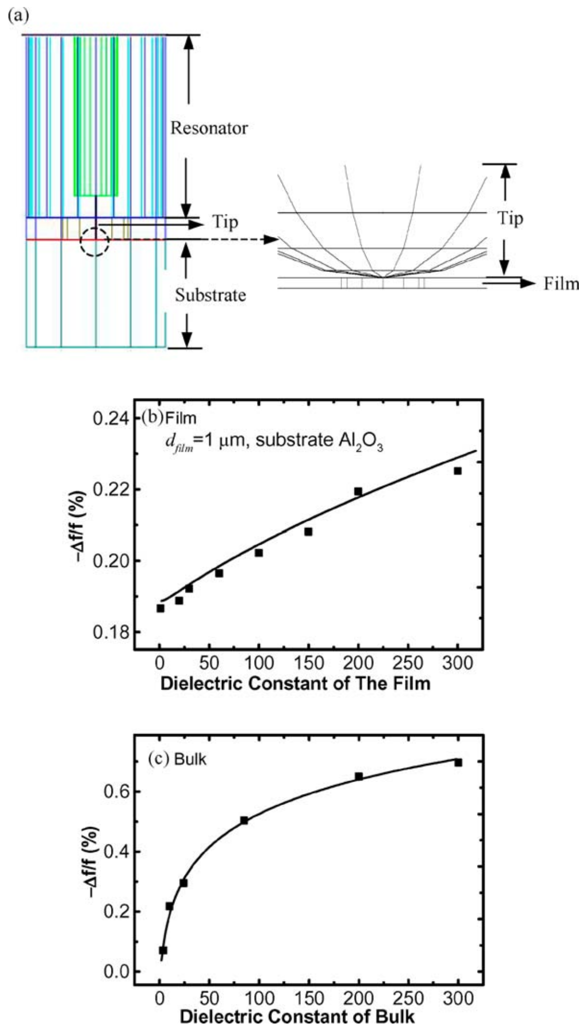

Fig. 1. (a) Geometry of EMP system used in finite element simulation; Frequency shifts versus dielectric constant data of (b) thin film and (c) bulk obtained from HFSS simulation (Tip radius: $R_0 \sim 35\ \mu$m).

element calculation of the electric and magnetic fields for a time-varying three-dimensional region. In this study, the frequency shifts of the measuring resonator were simulated using a 3D Ansoft HFSS v. 8 software package. Figure 1(a) also represents the model constructed for the simulation of the thin-film measurement in EMP system. It should be noted that the field intensity propagating out of the resonator decays exponentially, and can only penetrates into the samples for about 10–100 μm, depending on the tip radius and the dielectric constant of the sample. The higher the dielectric constant of the sample is, the shallower the penetration depth. The simulated frequency shift versus dielectric constant of the films for the EMP system with radius $R_0 = 30\ \mu$m is shown in Fig. 1(b), which illustrates the variation of frequency shift with the dielectric constant of the film is a continuous curve. The value of frequency shift is mostly determined by the dielectric constant of the substrate; however, the frequency shift $(-\Delta f/f)$ also increases slightly and monotonously with the dielectric constant of the films. By contrast, the simulated result for the bulk measurement shows the frequency shift varies significantly with the dielectric constant of the bulk (Fig. 1(c)). This phenomenon is due to the extremely small geometrical ratios of the films for the electric field distribution, as compared with those of the bulk samples. However, since the instrumental frequency sensitivity of EMP can be up to $\delta f/f \sim 10^{-6}$, the result in Fig. 1(b) reveals that EMP can be applied for thin-film measurement. Moreover, the dielectric constants of bulk samples analyzed from measured frequency response using curve in Fig. 1(c) are consistent with the measurements performed by conventional Hakki-Colemann method, indicating that the simulation is performed reasonably well.

The value of frequency shift can be even intensified by using conductive substrate. Due to the total reflection of the microwave at the conductive interface, the electric field inside the film is strongly amplified. Figure 2 shows the measured EMP frequency response curves of microwave dielectric BMT and ferroelectric PZT thin films deposited on Pt substrates.

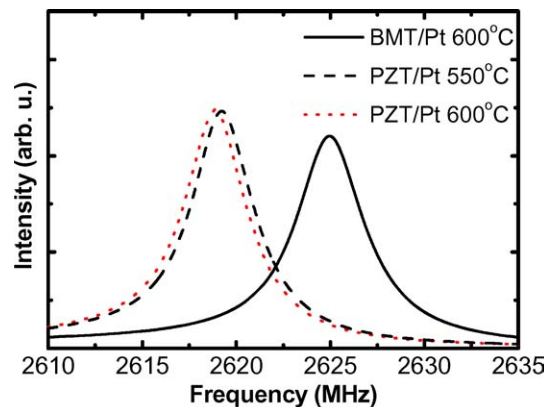

Fig. 2. EMP frequency response curves of (a) BMT/Pt thin films annealed at 600°C, (b) PZT/Pt thin films annealed at 550°C, and (c) PZT/Pt thin films annealed at 600°C.

The frequency shift ($-\Delta f/f$) increases from 0.26% for BMT film ($K \sim 25$) to about 0.53% for PZT films ($K \sim$ 500–600), which is more significant than the variation for the measurement of thin films deposited on Al_2O_3 substrate (Fig. 1(b)). The frequency response even reveals that the PZT films annealed at 600°C possess higher dielectric constant than those annealed at 550°C. This sensitive result also implies that the EMP technique possesses good capability of measuring tunable films in microwave frequency region.

To further investigate the causes of the dielectric behaviors of the films, the microstructure of the films were measured. Figure 3 shows the microstructure of the BMT/MgO films measured by atomic force microscope (AFM). The grains in the films are relatively small as compared with those in bulks. Figure 3(a) shows the BMT films are well crystallized with the average grain size of 200–300 nm, when the film is post-annealed at 600°C. Detailed examinations on the AFM images also reveal that the main matrices are BMT phases but there are still some unreacted particles existing in these samples. The AFM micrographs of PZT films post-annealed at 550 and 600°C are shown in Figs. 3(b) and (c), respectively. The PZT films post-annealed at 550°C (1 h) contain plate-like pyrochlore phase and some equi-axied particulates phases, indicating that part of the amorphous phase has been converted into perovskite phase (Fig. 3(b)). It needs at least 600°C to trigger the formation of perovskite phase for the PZT films. Figure 3(c) shows the grain size of the PZT films is about 100 nm.

The other powerful feature of EMP technique is mapping the distribution of dielectric properties of materials in very high spatial resolution. Figure 4 shows the mappings of resonant frequency of the BMT and PZT thin films. The high spatial resolution is obtained by using a sharp tip with radius about 5 μm. A sub-micrometer resolution is achieved, and the granular structure in size is observed even for the films. The frequency shifts in these images represent the microwave dielectric behavior of films in micro-scale region. As the result shown in Fig. 2, the PZT images (Figs. 4(b) and (c)) possess low resonant frequencies than the BMT images (Fig. 4(a)), since high dielectric constant of ferroelectric films will induce a large tip-sample capacitance in the equivalent circuit model. Most regions in PZT films annealed at 600°C even have higher dielectric constant (or lower resonant frequency) than those in the PZT films annealed at 550°C. Moreover, Fig. 4(b) shows the equi-axied particulates phases in AFM (Fig. 3(b)) possess higher dielectric constant than the amorphous matrix.

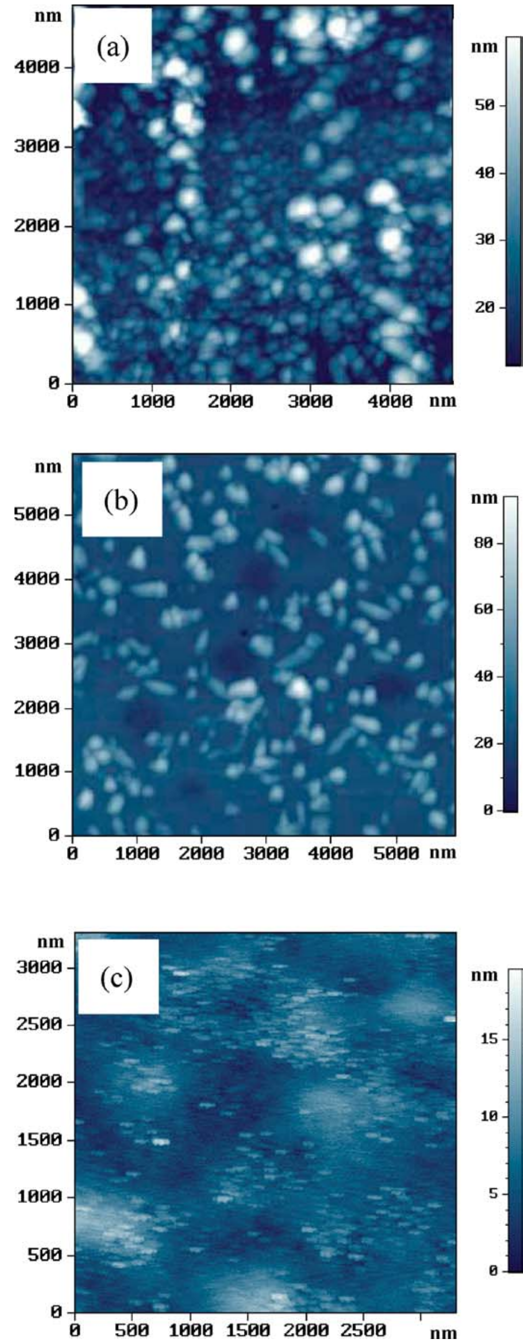

Fig. 3. AFM topographies of (a) BMT/Pt thin films annealed at 600°C, (b) PZT/Pt thin films annealed at 550°C, and (c) PZT/Pt thin films annealed at 600°C.

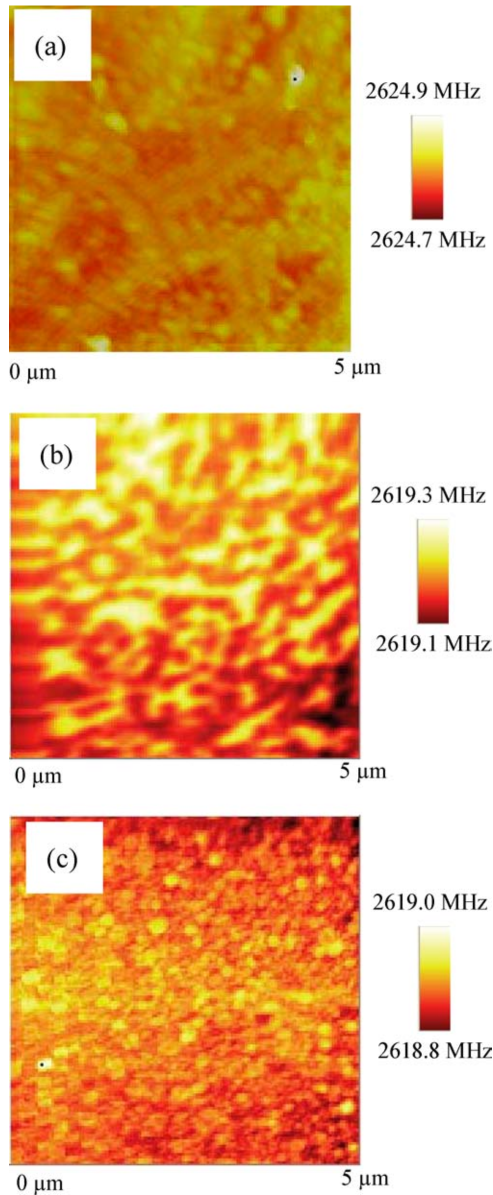

Fig. 4. EMP frequency images of (a) BMT/Pt thin films annealed at 600°C, (b) PZT/Pt thin films annealed at 550°C, and (c) PZT/Pt thin films annealed at 600°C.

4. Conclusions

The dielectric measurement of ferroelectric PZT and microwave dielectric BMT thin films were performed at microwave frequencies by introducing a microwave near field technique. The dielectric constants of the samples under test can be derived from the shift of resonant frequencies, which were modeled by a 3-dimensional finite element simulation. The dielectric images scanned are not only consistent with the AFM microphotos, but also the dielectric constant distribute differently between different samples. A sub-micron spatial resolution is achieved, and the grains of thin films can be resolved in the dielectric images. The results for ferroelectric and dielectric thin film measurements show high sensitivity and large applicable dielectric constant range, implying that the EMP technique possesses good capability for studying tunable properties of thin films in microwave frequency region.

Acknowledgment

Financial support of National Science Council, R.O.C., through the projects no. NSC 91-2622-E-007-027, NSC 91-2112-M-003-024 and NSC 92-2622-E-007-016, NSC 92-2210-E-003-001 is gratefully acknowledged by the authors.

References

1. B.H. Hoerman, G.M. Ford, L.D. Kaufmann, and B.W. Wessels, *Appl. Phys. Lett.*, **73**, 2248 (1998).
2. H.C. Li, W. Si, A.D. West, and X.X. Xi, *Appl. Phys. Lett.*, **72**, 190 (1998).
3. P. Kr. Petrov, E.F. Carlsson, P. Larsson, M. Friesel, and Z.G. Ivanov, *J. Appl. Phys.*, **84**, 3134 (1998).
4. Yu.A. Boikov and T. Claeson, *J. Appl. Phys.*, **81**, 3232 (1997).
5. T. Findikoglu, Q.X. Jia, and D.W. Reagor, *IEEE Transactions on Applied Superconductivity*, **7**, 2925 (1997).
6. S. Gevorgian, E. Carlsson, P. Linner, E. Kollberg, O. Vendik, and E. Wikborg, *IEEE Trans. Microwave Theory and Techniques*, **MTT-44**, 1738 (1996).
7. G. Vendik, E. Kollberg, S.S. Gevorgian, A.B. Kozyrev, and O.I. Soldatenkov, *Electronics Lett.*, **31**, 654 (1995).
8. C.H. Mulle, F.A. Miranda, S.S. Toncich, and K.B. Bhasin, *IEEE Transactions on Applied Superconductivity*, **5**, 2559 (1995).
9. E. Carlsson and S. Gevorgian, *Electronics Lett.*, **33**, 145 (1997).
10. A. Lahrech, R. Bachelot, P. Gleyzes, and A.C. Boccara, *Appl. Phys. Lett.*, **71**, 575 (1997).
11. Y. Lu, T. Wei, F. Duewer, Y. Lu, N.B. Ming, P.G. Schultz, and X.D. Xiang, *Science*, **276**, 2004 (1997).
12. G. Chen, T. Wei, F. Duewer, Y. Lu, and X.D. Xiang, *Appl. Phys. Lett.*, **71**, 1872 (1997).
13. C. Gao, F. Duewer, and X.D. Xiang, *Appl. Phys. Lett.*, **75**, 3005 (1999).
14. Y.C. Chen, H.F. Cheng, G. Wang, X.D. Xiang, C.M. Lei, and I.N. Lin, *Jpn. J. Appl. Phys.*, **41**, 7214 (2002).
15. S. Nomura, K. Toyama, and K. Kaneta, *Jpn. J. Appl. Phys. Part 2*, **21**, L624 (1982).
16. R. Guo, A.S. Shalla, and L.E. Cross, *J. Appl. Phys.*, **75**, 4704 (1994).